Thin Solid Films 527 (2013) 179–185

Contents lists available at SciVerse ScienceDirect

Thin Solid Films

journal homepage: www.elsevier.com/locate/tsf

Reversible wettability control of silicon nanowire surfaces: From superhydrophilicity to superhydrophobicity

Jungmok Seo [a], Soonil Lee [a], Heetak Han [a], Youngwon Chung [a], Jaehong Lee [a], Sung-Dae Kim [b], Young-Woon Kim [b], Sangwoo Lim [c], Taeyoon Lee [a,*]

[a] Nanobio Device Laboratory, School of Electrical and Electronic Engineering, Yonsei University, 134 Shinchon-Dong, Seodaemun-Gu, Seoul 120-749, Republic of Korea
[b] In-situ Electron Microscopy Laboratory, Seoul University, Gwanakro 599, Dae-Hak Dong, Gwanak-Gu, Seoul 151-744, Republic of Korea
[c] Department of Chemical and Biomolecular Engineering, Yonsei University, 134 Shinchon-Dong, Seodaemoon-Gu, Seoul 120-749, Republic of Korea

ARTICLE INFO

Article history:
Received 4 June 2012
Received in revised form 7 December 2012
Accepted 7 December 2012
Available online 19 December 2012

Keywords:
Water adhesive surface
Siloxane formation
Superhydrophobic
Si nanowire
Metal assisted chemical etching
Wettability conversion

ABSTRACT

Bio-inspired superhydrophobic surfaces have attracted considerable attention due to their potential applications. Although various techniques to fabricate artificial superhydrophobic surfaces have been demonstrated, most of the methods lack water adherence or controllable wetting properties of the surfaces, which hinders their practical usage. In this paper, we present a simple approach to fabricate water-adhesive superhydrophobic silicon nanowire (Si NW) surfaces by applying a thermal annealing treatment in oxygen ambient. The Si NW arrays were fabricated using a metal assisted chemical etching method. After the cycled rapid thermal annealing (RTA) process at 1000 °C under oxygen ambient, the water contact angle of the Si NW surface changed dramatically from 0 to 154.3° with high water-adhesive properties. This drastic change of the wettability could be attributed to the formed siloxane groups (—Si–O–Si–) on the thermally-treated Si NW surfaces; H_2O is released from two adjacent silanol groups (–Si–O–H) to form siloxane groups during the RTA process. When the annealed Si NW was exposed in air, the wettability of the superhydrophobic Si NW was reconverted due to the re-formation of silanol groups (–Si–O–H). The wettability conversion of Si NW between superhydrophilic and superhydrophobic was repeated with good reversibility.

1. Introduction

Artificial superhydrophobic surfaces (water contact angle (*CA*) > 150°) have received much attention for various potential applications ranging from self-cleaning to oil spill clean-up [1–6]. The extreme wetting property was often obtained by tailoring the surface energy of micro- or nano-structured surfaces [7–9]. Particularly, in order to realize the superhydrophobic surfaces, the increment of the surface roughness is more significant than modification of the surface energy since the maximum achievable water *CA* on a flat surface with a coated layer with the lowest surface energy is only 119° [10]. Superhydrophobic surfaces can be categorized into two states according to their droplet adhesive properties. When the water *CA* hysteresis (advancing *CA*–receding *CA*) is below 10°, the superhydrophobic surfaces are considered to be in the Cassie wetting regime, which exhibit self-cleaning and water repellent characteristics. On the contrary, superhydrophobic surfaces with a water *CA* hysteresis larger than 10° are in the Wenzel wetting regime, which show water-adhesive property [11,12]. Recently, these Wenzel wetting surfaces have been actively researched where water droplets could be firmly pinned with a nearly spherical shape since they can be applied to advanced microfluidic applications such as liquid transporting systems, biochemical separation, and single-molecule spectroscopy [13–16].

Superhydrophobic surfaces with water-adhesive property have been demonstrated using various organic and inorganic materials including polystyrene [17], aluminum alloys [18], a mixture of poly (methyl methacrylate) and amphiphilic polyurethane [19], and titanium oxide (TiO_2) [20]. Although the aforementioned methods produce highly water-adhesive superhydrophobic surfaces, they require complex processes to obtain the micro- or nano-structures combined with chemically functionalized surfaces with a low surface energy. In addition, the wetting properties of the demonstrated surfaces cannot be manipulated from superhydrophilic (water *CA* < 5°) to become superhydrophobic and are not reversible.

Here, we demonstrate a method to obtain superhydrophobic surfaces with a high water-adhesive property via simple surface modification of Si nanowire (NW). The vertically-aligned high-dense Si NW arrays were fabricated using metal assisted chemical etching (MACE) method. The surface of the as-fabricated Si NW exhibiting superhydrophilic wetting properties could be modified to become a superhydrophobic surface with a static water *CA* of 154.3° by means of 10 cycles of rapid thermal annealing (RTA) at 1000 °C in oxygen ambient. The extreme wettability change of the Si NW is supposed to be due to the decreased surface energy of the Si NW induced by the conversion of silanol groups (–Si–O–H) into siloxane groups (–Si–O–Si–)

* Corresponding author. Tel.: +82 2 2123 5767; fax: +82 02 313 2879.
E-mail address: taeyoon.lee@yonsei.ac.kr (T. Lee).

0040-6090/$ – see front matter © 2012 Elsevier B.V. All rights reserved.
http://dx.doi.org/10.1016/j.tsf.2012.12.010

by releasing of H_2O from two adjacent silanol groups during the annealing treatment. The wettability of the Si NW was gradually re-converted from superhydrophobic to superhydrophilic when the samples were stored under ambient conditions due to the re-formation of silanol groups on the surface of the Si NW, resulting in an increase of the surface energy. Within our experiment range, the wettability of the Si NW could be reversibly switched by alternation of the cycled RTA process and air storage.

2. Experimental procedure

2.1. Fabrication of vertically aligned Si NW arrays

Vertically aligned Si NW arrays were obtained using the MACE method and the details are described elsewhere [21–23]. The (100) oriented p-type Si wafers (1–10 Ω·cm) were successively rinsed with acetone, isopropyl alcohol, and de-ionized water. Subsequently, the native oxide removal process was carried out by immersing the substrate in a 5% HF aqueous solution for 3 min at room temperature. The cleaned substrate was immediately dipped into an aqueous solution containing 30 mM $AgNO_3$ and 4.9 M HF at 70 °C for various etching times (t_e). The undesired by-products (silver dendrites and silver nanoparticles) generated during the NW fabrication process were removed by successive rinsing with a 30 wt.% HNO_3 aqueous solution. The removal of the oxide layer and H-termination on the surface of the Si NW was carried out by dipping the Si NW in 5 wt.% HF for 3 min, followed by cleaning with de-ionized water at room temperature.

2.2. Surface treatments of Si NW

To modify the surface of the as-fabricated Si NW, the RTA process was carried out at 1000 °C for 10 cycles under oxygen ambient where the pressure was maintained at 13.3 Pa. In each cycle, the temperature of the chamber was ramped up under N_2 ambient for 65 s followed by the annealing process under O_2 ambient at 1000 °C for 30 s and then rapidly cooled down under a vacuum ambient. The same surface treatment process was also carried out on a flat Si substrate as a reference.

To compare the wettability changes caused by different surface treatments, H-terminated, ~30% F and ~70% H-terminated, and dodecyltrichlorosilane (DTS)-coated substrates for both flat Si and Si NW were prepared. To obtain H-terminated substrates, the as-prepared samples were dipped into a Teflon beaker containing a 49 wt.% HF solution for 3 min. Reaction of the H-terminated samples with liquid anhydrous methanol at 65 °C for 12 h led to ~30% methoxy-terminated surfaces. Then, the ~30% methoxyl-terminated surfaces were immersed in a 49 wt.% HF solution for 3 min where the methoxyl groups were altered by the fluoride groups, resulting in ~30% F and ~70% H-terminated substrates. The DTS-coated substrates were obtained by immersing the flat Si and Si NW samples in a 3 mM solution of DTS dissolved in hexane for 30 min at room temperature. The samples were cleaned with ethanol and then subjected to a baking process at 150 °C for 1 h to obtain a dense DTS layer.

2.3. Surface characterization

The surface morphologies of the Si NW were characterized using a JEOL JSM-6360 field emission scanning electron microscope (FE-SEM) and a FEI Tecnai F20 high resolution transmission electron microscope (HR-TEM) with operating voltages of 10 kV and 200 kV, respectively. For TEM analysis, Si NW were cut using surgical blade and dispersed in ethyl ethanol, followed by ultrasonication for 30 s. The Si NW solution was then dropped onto carbon films on copper grids. Fourier transform infrared (FTIR) spectra were measured using a Bruker Vertex 70 spectrometer equipped with an attenuated total reflection accessory in the range of 400 to 4000 cm^{-1}. Water *CA* measurements were carried out using ~5 μL droplets of de-ionized water with a *CA* instrument (Phoenix 300, SEO Co. Ltd.) equipped with a dynamic image capture camera.

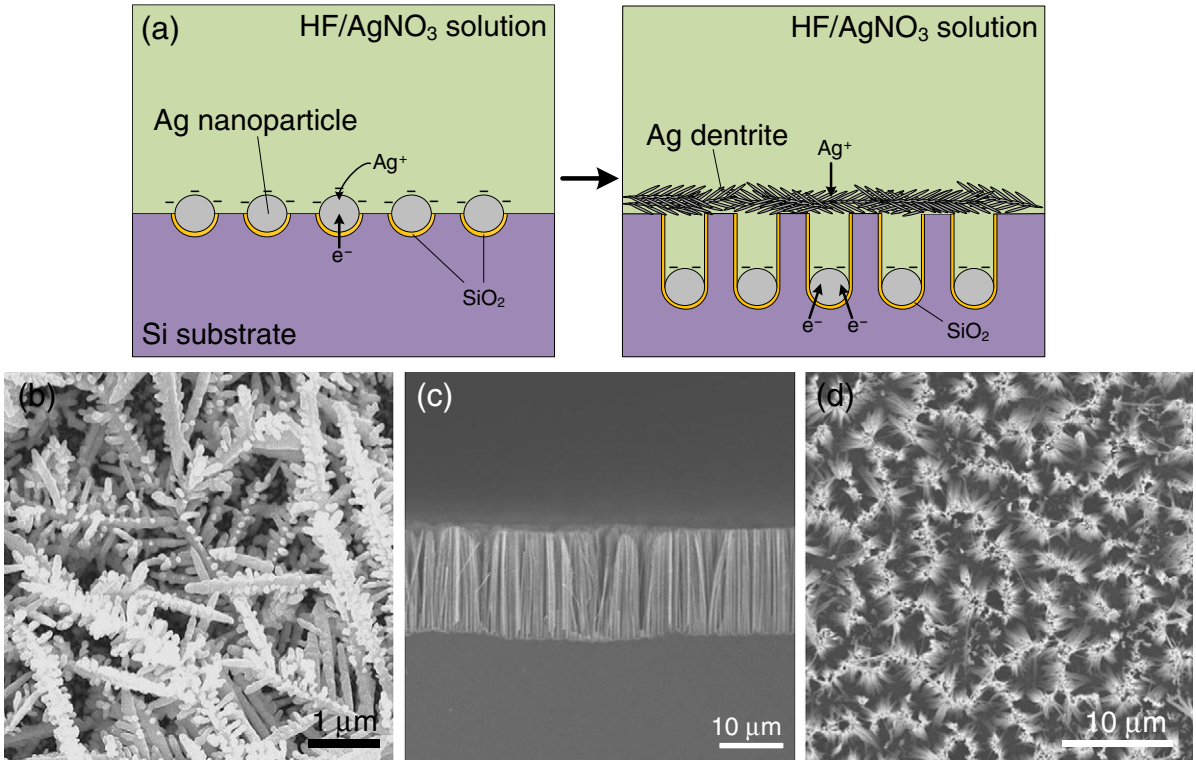

Fig. 1. (a) A schematic of the fabrication mechanism of Si NW arrays on the Si surface in an aqueous $HF/AgNO_3$ solution. (b) SEM image of silver dendrites branched at the top surface of a Si substrate. (c) Typical SEM cross-sectional image of fabricated Si NW arrays. (d) Typical top-view SEM image of the fabricated Si NW arrays.

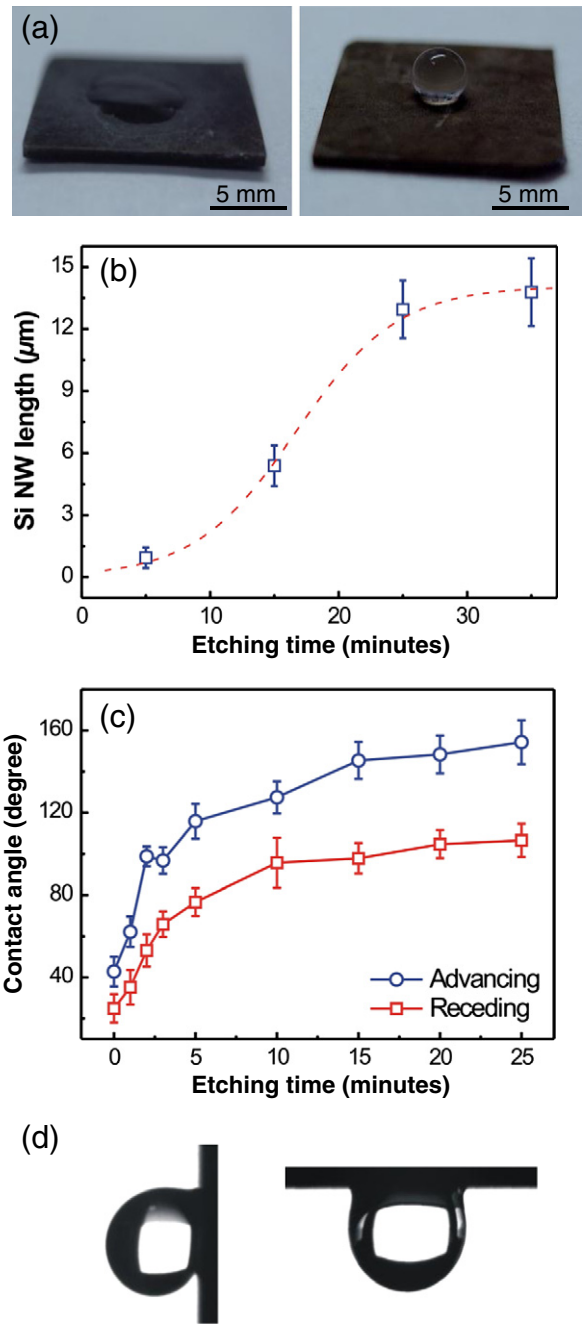

Fig. 2. (a) Photographs of a water droplet on the as-fabricated (left) and cycled RTA-treated Si NW with a t_e of 25 min. (b) The length of the fabricated Si NW as a function of t_e. (c) Advancing and receding water *CA* values of the cycled RTA-treated Si NW as a function of t_e. The circle symbols represent the advancing *CA* results and the square symbols represent the receding *CA* values. (d) Photographs of a water droplet on cycled RTA-treated Si NW at different tilt angles of 0° (left), 90° (middle), and 180° (right).

3. Results and discussion

Fig. 1(a) shows a schematic of the mechanism of the MACE method used to fabricate the vertically aligned Si NW arrays. The formation of the Si NW can be ascribed to the electrochemical reactions of the Si substrate in the solution mixture of $AgNO_3$ and HF. When the Si substrate is dipped into the solution, Ag^+ ions near the surface obtain electrons from the valance band of Si and the Ag ions are deposited on the surface in the form of Ag nanoparticles. Since the deposited Ag nanoparticles on the Si surface are more electronegative than Si, they strongly attract electrons from Si which lead to the negatively charged nanoparticles [24]. These charged Ag nanoparticles act like catalysts which induce subsequent reduction of Ag^+ ions in solution and facilitate Si oxidation at the interface between the Si and Ag nanoparticles, as shown in the left schematic in Fig. 1(a). As the reaction proceeds, more Ag^+ ions are deposited around the nanoparticles and further oxidation simultaneously occurs at the Si beneath the Ag nanoparticles. The generated SiO_2 layer at the interface is subsequently etched by the HF solution and this sequential oxidation and etch process create highly dense etch pits. Some large Ag nanoparticles which could not enter the etch pits form silver dendrites on the top surface of the substrate, as shown in the right schematic in Fig. 1(a). With increasing immersion time, the produced silver dendrites cover the entire surface, blocking the additional deposition of Ag into the etch pits. An SEM image of silver dendrites produced on the top of the surface is shown in Fig. 1(b). Fig. 1(c) and (d) are typical SEM cross-sectional and top-view images, respectively, of Si NW fabricated on a Si substrate using the MACE method with a t_e of 25 min. As shown in Fig. 1(c), it was observed that the obtained Si NW arrays were vertically aligned over a large area with uniform lengths (~14 μm) and diameters ranging from 100 to 150 nm. In addition, the vertically aligned Si NW arrays formed Si NW bundles at their tips, as shown in Fig. 1(d). The formation of Si NW bundles may be ascribed to the capillary force of the liquid during the drying process of the substrate.

The water *CAs* of the as-fabricated and cycled RTA-treated Si NW were evaluated to identify the effect of the thermal treatment process under oxygen ambient on the wettability of the Si NW. Interestingly, the wettability of the Si NW with a t_e of 25 min was drastically changed from superhydrophilic (left image of Fig. 2(a)) to superhydrophobic (right image of Fig. 2(a)) by the cycled RTA treatment. To investigate the structural effects on the wettability change of the RTA-treated Si NW, the water *CA* values were measured by varying the length of the Si NW. The length of the Si NW can be adjusted by varying t_e. Fig. 2(b) exhibits the relationship between the length of the fabricated Si NW and t_e where the length of the Si NW increased proportionally with increasing t_e. The average length of the NW increased from 0.94 to 14.8 μm as t_e was increased from 5 to 35 min and the etching rate of Si becomes saturated when t_e is greater than 25 min. Fig. 2(c) shows the measured advancing and receding *CAs* of the water droplets on the cycled RTA-treated Si NW as a function of t_e. The water *CAs* were measured at five different locations on the substrate and then averaged. As the length of the Si NW increased, the surface roughness of the substrate increased and the resulting wettability of the cycled RTA-treated Si NW changed from the hydrophilic regime ($CA<90°$) to the superhydrophobic regime ($CA>150°$). The *CA* hysteresis, differences between the advancing and receding *CA*, were relatively large (>21°) over the entire samples within our experimental ranges (t_e varied from 1 to 25 min). Specifically, when $t_e \geq 20$ min, the resulting static water *CAs* were larger than 150° and the values of the water *CA* hysteresis were larger than 48°. The relatively large water *CA* hysteresis on the superhydrophobic Si NW indicates that the demonstrated superhydrophobic surface can be regarded as possessing water-adhesive properties, where a water droplet did not slide even when the substrate was tilted vertically (left image of Fig. 2(d)) and turned upside down (right image of Fig. 2(d)). It is noteworthy that there were no significant morphological changes on the Si NW before and after the RTA process under oxygen ambient. This interesting phenomenon of the high water-adhesive superhydrophobic surface is distinct from other previous reports of superhydrophobic surfaces with a strong water repellent property, which showed 'roll off' characteristics [25,26]. The demonstrated superhydrophobic surface with water pinning characteristics can be explained by the Wenzel state model [9]. In this model, the contact area between the liquid and surfaces, which is related to the surface roughness, determines the wettability of the surface, as shown in the following equation:

$$\cos\theta_c = r\ \cos\theta, \tag{1}$$

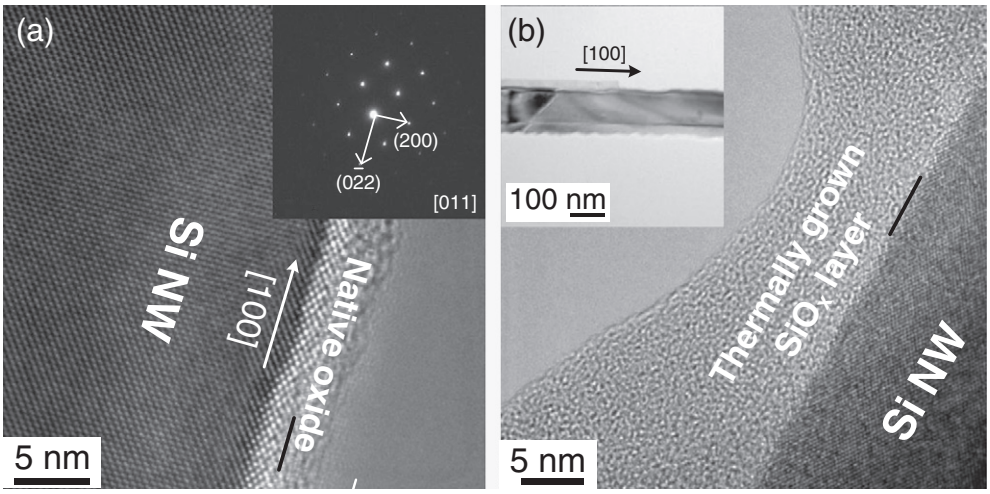

Fig. 3. High resolution bright-field TEM micrographs of (a) as-fabricated Si NW (the inset shows its electron diffraction pattern taken along the [011] zone axis) and (b) cycled RTA-treated Si NW. The inset shows a low-resolution TEM micrograph.

where r is the ratio between the actual surface area of a rough surface and its projected surface area, θ_c is the measured *CA* on a rough surface, and θ is the intrinsic *CA* on a flat surface. The Wenzel state model assumes that the contact line between a rough surface and liquid follows all of the topological variations of the surface. Thus, the interface between air and the surface gets replaced with a solid and liquid interface with the same surface area. Consequently, the droplet wets the rough surface and this wetting creates a large contact area between the droplet and the surface, giving rise to firm pinning of the water droplet on the surface.

To examine the change of the surface in an individual Si NW after the post-cycled RTA treatment, TEM analyses were carried out. Fig. 3(a) shows a typical HR-TEM micrograph of an as-fabricated Si NW, taken along the [011] zone axis where the inset is the corresponding electron diffraction pattern. As shown in Fig. 3(a), the as-fabricated Si NW exhibited a fairly smooth surface and was wholly covered with a 2.4 ± 0.4 nm thick native oxide layer. The contour of the outermost surface followed the surface of the bare Si NW and the Si NW covered with the native oxide layer also showed a fairly smooth surface. The cycled RTA process was adopted in the high temperature RTA process under oxygen ambient to maximize the surface oxidation rate of the Si NW. In the initial stage of oxidation, the thickness of the grown oxide layer increased linearly. However, it was reported that the formation of positive fixed charges near the interface between Si and SiO_x could decrease the oxidation rate as the oxidation process proceeds [27,28]. The formed fixed charges could be reduced by the N_2 gas flowing during the ramping up of the annealing temperature in the cycling RTA process [29,30]. Fig. 3(b) shows a representative HR-TEM micrograph of the surface of the cycled RTA-treated Si NW and the inset image shows a low-resolution TEM micrograph image. It is clearly observed that the SiO_x layer was thermally grown on the surface of the Si NW via the cycled RTA process with a thickness $\geq$~9 nm. The thermally grown oxide layer was much thicker than the native oxide layer of the as-fabricated Si NW. In addition, the outermost surface roughness was significantly increased. The increment of the outermost surface roughness could be attributed to the uneven oxidation rate and the volume difference between Si and SiO_x. Si atoms at convex regions of the rough surface of the as-fabricated Si NW experience a faster oxidation rate than at concave regions since a larger localized amount of Si atoms could be supplied to form SiO_x at convex regions than the amount of Si atoms at the concave regions. The uneven oxidation rate led to the reduced interface roughness between the Si and SiO_x layer. In addition, the volume of SiO_x is larger than the volume of Si atoms, causing a further increment of the outermost surface roughness.

However, the roughed surface of the outermost Si NW cannot fully explain the drastic wettability change of the Si NW. In general, the increased surface roughness of the hydrophilic surface leads to a more hydrophilic surface in the Wenzel state [9]. In the present case, the outermost roughness of the RTA-treated Si NW was significantly increased based on the TEM analyses. According to the measured water *CA* data, the wettability of the RTA-treated Si NW surface drastically changed from superhydrophilic to superhydrophobic. Considered the observed phenomenon, the surface wettability of the Si NW may be changed from hydrophilic to hydrophobic during the cycled RTA process. The changes of the surface energy can be elucidated by the formation of hydrophobic siloxane groups, by releasing a water molecule of two adjacent surface hydrophilic silanol groups at the Si NW surfaces [31–34]. Fig. 4(a) shows a schematic illustration of the ion adsorption process on the surface of the Si NW. At the surface of the as-fabricated Si NW, hydroxyl ions (OH^-) are prone to be chemisorbed on the dangling bonds and surface defects of the Si NW, leading to the formation of silanol groups [35]. The hydrophilic nature of the silanol groups on as-fabricated Si NW surfaces results in superhydrophilicity. However, during the post thermal annealing process in oxygen ambient, most of the hydroxyl groups on the Si NW surface could be altered to siloxane groups by releasing H_2O from two adjacent silanol groups. Since the siloxane groups are not strained, the siloxane groups do not easily hydrolyze to form hydrogen bonds with the oxygen molecules in water. Hence, the wettability of the RTA-treated Si NW was converted from hydrophilic to hydrophobic [36]. To verify the effects of the gas ambient present during the cycled RTA process, the same annealing process was carried out under various ambient conditions including vacuum, nitrogen, air, and hydrogen ambient. After the RTA process under vacuum, air, and nitrogen ambient, the water *CA*s were slightly increased (from nearly 0 to ~10°) due to the dehydration which enhances the formation of siloxane groups at the Si NW surface. However, the wettability of the RTA-treated Si NW was not changed from hydrophilic to hydrophobic and wettability of the Si NW was re-converted to superhydrophilicity (water *CA* ~0°) within few minutes, which could indicate that the amount of formed siloxane groups was small and not enough to convert the wettability of cycled RTA-treated Si NW from hydrophilic to hydrophobic. Under hydrogen ambient RTA process, the structure of the Si NW arrays was damaged due to the surface self-diffusion of Si atoms during the high-temperature thermal annealing process [37,38].

When the RTA-treated Si NW in oxygen ambient were placed under atmospheric conditions for tens of minutes, the wettability of the Si NW was re-converted from superhydrophobic to superhydrophilic since the

siloxane group is energetically stable only at the high temperature [36,39]. We assume that the siloxane groups formed on the Si NW are gradually replaced with silanol groups on the defect sites and dangling bonds of the Si NW. Fig. 4(b) exhibits the wettability changes of a single droplet on the cycled RTA-treated Si NW as a function of time. The water droplets were dropped on different locations of the same sample for each measurement and the measurement time interval was 10 min. As shown in Fig. 4(b), the re-formation of hydroxyl groups on the RTA-treated Si NW surface actively proceeded at the initial stage (from 0 to 10 min) and the re-formation rate gradually decreased as time increased. After 50 min, the wettability of the RTA-treated Si NW was fully re-converted from superhydrophobic to superhydrophilic. In addition to obtaining the *CA* measurements from different locations of a sample as a function of time, the change of the *CA* of a single droplet at a fixed location was also measured over time. It was observed that when a water droplet was in direct contact with the surface of the Si NW, the wettability change from superhydrophobic to superhydrophilic took place much faster than when the sample was placed under ambient conditions where it required approximately 12 min. This is probably due to the enhanced re-formation rate of hydroxyl groups on the surface of the Si NW, supplied directly from the oxygen molecules of the water droplet. To characterize the formation of siloxane groups on the RTA-treated Si NW in oxygen ambient, FTIR measurement was carried out. Fig. 4(c) and (d) shows typical FTIR spectra measured from the as-fabricated, cycled RTA-treated, and 1-hour-air-storaged Si NW after the cycled RTA treatment. As shown in Fig. 4(c), after the RTA process, two noticeable peak features appeared at ~888 and 908 cm^{-1}. These peaks correspond to siloxane groups which could also be found in previously reported dehydrated SiO_2 thin films induced by high-temperature annealing [31]. The large distortion of O–Si–O and Si–O–Si bond angles of the formed siloxane groups resulted in infrared active ring vibration mode and peak features at the FTIR spectra [40,41]. Notably, the peaks of the FTIR spectra were relatively broad compared to those of reference [31], since the FTIR measurement system used in our experiments were not directly interfaced to a RTA vacuum chamber system; the formed siloxane groups could be altered to silanol groups by adsorption of water molecules in ambient conditions. After storing in air, the peaks related to siloxane groups disappeared. On the contrary, as shown in Fig. 4(d), the broad peak related to silanol bonds (wavelength of ~3000 to 3500 cm^{-1}) of as-fabricated Si NW was decreased after the RTA treatment as H_2O molecule was released from two adjacent silanol groups. After air storage for 1 h, the peak was restored which indicates the re-formation of silanol groups on the Si NW surfaces.

Fig. 5(a) shows photographic images of water droplets on as-fabricated (left) and cycled RTA-treated (right) Si NW. On the as-fabricated Si NW, the measured water contact angle was nearly zero, indicating that the resulting surface was superhydrophilic. On the other hand, the cycled RTA-treated Si NW showed superhydrophobicity with a maximum water *CA* of 154.3°. Fig. 5(b) shows the reversible extreme wettability conversions of the Si NW between superhydrophilic and superhydrophobic via the formation of silanol and siloxane groups on the surface of the Si NW, indicating the good reversibility of the surface wettability conversion within our experimental ranges (4 times). Notably, there were no significant changes in the measured water *CA*s in the repeated hydrophobic and hydrophilic states, although the outmost surface roughness of the individual Si NW increased substantially during the repeated cycles of the RTA treatment. Hence, it can be inferred that the drastic change in the wettability of the Si NW was mainly affected by the siloxane group formation on the Si NW surfaces rather than the surface roughness of the Si NW.

To compare the wettability changes caused by the different surfaces treatments, static water *CA*s were measured on the surfaces of both flat Si and Si NW samples terminated with H, ~30% F and ~70% H, dodecyltrichlorosilane (DTS) alkyl chains, and siloxane groups. Fig. 6 shows the obtained values of the static water *CA*s on the various

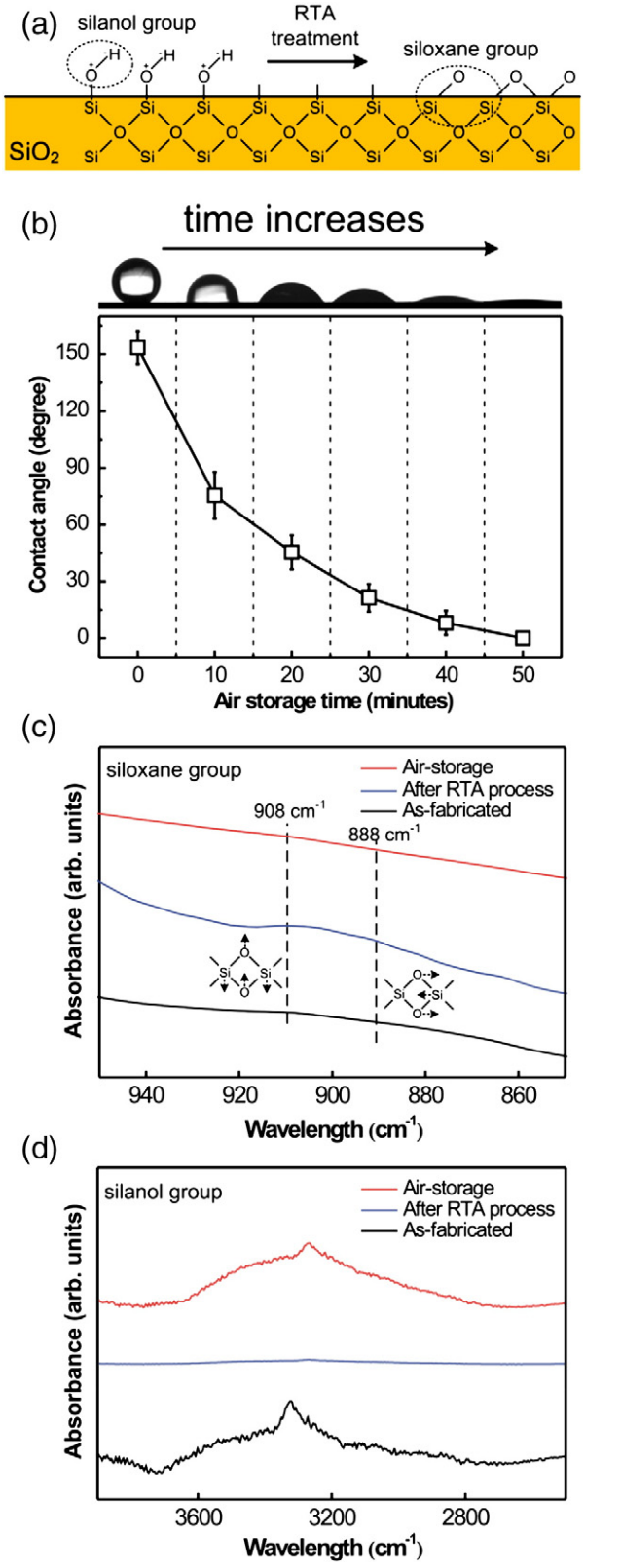

Fig. 4. (a) A schematic of the hydrophilic (silanol) and hydrophobic (siloxane) groups formed on Si NW covered with SiO_2. (b) An optical photographic image of a water droplet on cycled RTA-treated Si NW (top) and the changes of the water *CA* as a function of time (bottom). (c) Absorption infrared spectra from 950 to 850 cm^{-1} for as-fabricated, RTA-treated, 1-hour-air-stored Si NW. (d) Absorption infrared spectra from 3950 to 2950 cm^{-1} for as-fabricated, RTA-treated, 1-hour-air-stored Si NW.

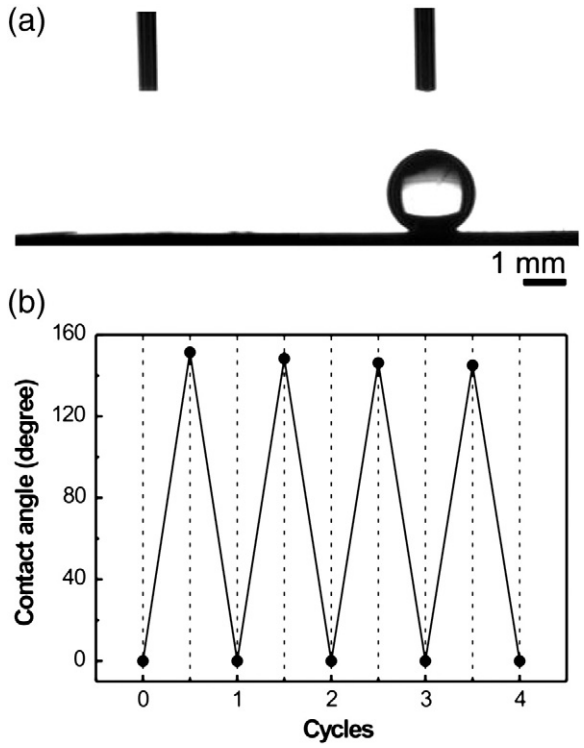

Fig. 5. (a) Photographs of water droplets on the as-fabricated (left) and cycled RTA-treated (right) Si NW surfaces. (b) Reversible superhydrophilic–superhydrophobic conversion of the Si NW.

surface-treated flat Si and Si NW substrates. On the bare Si substrate, the measured water *CA* was $45 \pm 6.4°$. Compared to the Si substrate, the water *CAs* increased slightly after the various surface treatments due to the lowered surface energy. The RTA-treated flat Si substrate showed relatively small increment of water *CA* (from ~45 to 61°), and the wettability was not changed to hydrophobic. The ~30% F and ~70% H-terminated Si substrate showed a larger water *CA* than the H-terminated flat Si substrate since the F-terminated surface has a lower surface energy than the H-terminated surface [42]. At the flat surface, the water *CAs* (θ) can be determined by applying Young's equation as follows:

$$\cos\theta = (\gamma_{SV} - \gamma_{SL})/\gamma, \quad (2)$$

where γ is the liquid–vapor surface tension, γ_{SV} is the solid-vapor surface tension, and γ_{SL} is the solid–liquid surface tension. The DTS-coated Si substrate showed the lowest surface energy with a calculated value of 40.37 mN/m, assuming that the surface tension of water is 71.8 mN/m.

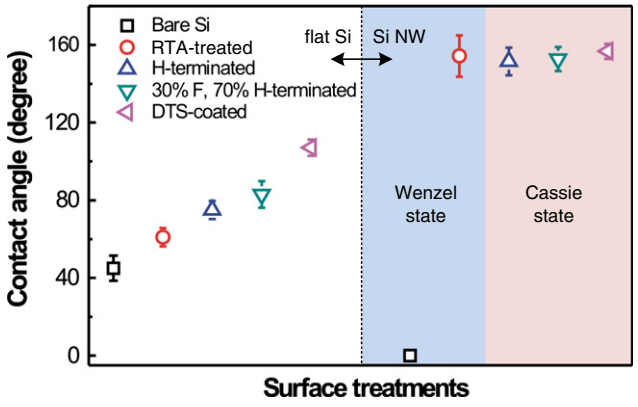

Fig. 6. Static water *CAs* measured on various surface-treated flat Si and Si NW.

On the Si NW, the surface wettabilities were drastically changed from superhydrophilic to superhydrophobic after the various surface treatments due to the rough structure formed on the surface. In the nanostructured surface, the wettability is known to be more dependent on the roughness of the surface than surface energy, and thus no substantial differences could be obtained in the water *CAs* measured from surface-treated Si NW. Notably, the RTA-treated Si NW showed high water-adhesive properties which indicates that the resulting surface follows the Wenzel state model while the other surface-treated surfaces exhibited high water repellent properties and roll-off characteristics, as detailed by the Cassie state model. We believe that the water-adhesive properties of the RTA-treated Si NW surface can be attributed to a small portion of the re-formed silanol groups on the post-treated NW. The hydrophilic silanol groups are energetically favorable compared to siloxane groups at room temperature. Thus, it can be inferred that a small amount of hydrophilic silanol groups are re-formed on the surface of the RTA-treated Si NW after the RTA treatment. The dominant hydrophobic siloxane groups strongly repel water [33,34], contributing to the water *CAs* being larger than 150°. On the contrary, a small portion of hydrophilic silanol groups on the surface of the RTA-treated Si NW attract the water droplet due to the interaction of hydrogen bonding between silanol groups and water molecules. A water-adhesive superhydrophobic surface with a small hydrophilic portion and a dominant hydrophobic region has been demonstrated using wettability controlled polyurethane [18]. The mechanism of the water-adhesive superhydrophobic surface is reasonably well understood theoretically and is thought to be adapted in our system in which the strong water-repulsion of hydrophobic siloxane groups and strong water-adhesion of hydrophilic silanol groups could result in the superhydrophobic surface with adhesion to water.

4. Conclusion

In summary, we demonstrated a facile method to create a high water-adhesive superhydrophobic Si NW surface. Si NW arrays were fabricated using the MACE method and their surface wettability could be drastically changed from superhydrophilic (water *CA* ~0°) to superhydrophobic (water *CA* ~154°) by the cycled RTA process under oxygen ambient. The obtained superhydrophobic Si NW surface showed water-adhesive characteristics, which could be explained by the Wenzel state model. On the superhydrophobic Si NW surface, dropped water droplets were pinned at the surface even when the substrate was tilted vertically and turned upside down. The wettability change is supposed to be due to the formation of siloxane groups on the dangling bonds and defects of the Si NW surface. The formed siloxane groups were altered to silanol groups when the cycled RTA-treated Si NW were stored in air ambient since the re-formation of hydroxyl ions and the formation of silanol groups are energetically favorable.

Acknowledgment

This research was supported in part by the Converging Research Center Program through the Ministry of Education, Science and Technology (2012K001321) and by the Priority Research Centers Program through the National Research Foundation of Korea (NRF) funded by the Ministry of Education, Science and Technology (2012–0006689). This work was also supported by National Research Foundation of Korea (NRF) grant funded by the Korean government (MEST) (no. 2011-0028594).

References

[1] L. Feng, S. Li, Y. Li, H. Li, L. Zhang, J. Zhai, Y. Song, B. Liu, L. Jiang, D. Zhu, Adv. Mater. 14 (2002) 1857.
[2] J. Seo, S. Lee, J. Hee, T. Lee, ACS Appl. Mater. Interfaces 3 (2012) 4722.
[3] A. Nakajima, A. Fujishima, K. Hashimoto, T. Watanabe, Adv. Mater. 11 (1999) 1365.
[4] T. Sun, L. Feng, X. Gao, L. Jiang, Acc. Chem. Res. 38 (2005) 644.

[5] R. Blossey, Nat. Mater. 2 (2003) 301.
[6] J. Yuan, X. Liu, O. Akbulut, J. Hu, S.L. Suib, J. Kong, F. Stellacci, Nat. Nanotechnol. 3 (2008) 332.
[7] X. Feng, L. Jiang, Adv. Mater. 18 (2006) 3063.
[8] N.J. Shirtcliffe, G. McHale, M.I. Newton, C.C. Perry, F.B. Pyatt, Appl. Phys. Lett. 89 (2006) 104106.
[9] Y. He, C. Jiang, H. Yin, W. Yuan, Appl. Surf. Sci. 257 (2011) 7689.
[10] T. Nishino, M. Meguro, K. Nakamae, M. Matsushita, Y. Ueda, Langmuir 15 (1999) 4321.
[11] R.N. Wenzel, Ind. Eng. Chem. 28 (1936) 988.
[12] A.B.D. Cassie, S. Baxter, Trans. Faraday Soc. 40 (1944) 546.
[13] X. Song, J. Zhai, Y. Wang, L. Jiang, J. Phys. Chem. B 109 (2005) 4048.
[14] L. Feng, Y. Zhang, J. Xi, Y. Zhu, N. Wang, F. Xia, L. Jiang, Langmuir 24 (24) (2008) 4114.
[15] A. Winkleman, G. Gotesman, A. Yoffe, R. Naaman, Nano Lett. 8 (2008) 1241.
[16] J.R. Dorvee, A.M. Derfus, S.N. Bhatia, M.J. Sailor, Nat. Mater. 3 (2004) 896.
[17] M. Jin, X. Feng, L. Feng, T. Sun, J. Zhai, T. Li, L. Jiang, Adv. Mater. 17 (2005) 1977.
[18] Z.G. Guo, W.M. Liu, Appl. Phys. Lett. 90 (2007) 223111.
[19] N. Zhao, Q. Xie, X. Kuang, S. Wang, Y. Li, X. Lu, S. Tan, J. Shen, X. Zhang, Y. Zhang, J. Xu, C.C. Han, Adv. Funct. Mater. 17 (2007) 2739.
[20] Y. Lai, C. Lin, J. Huang, H. Zhuang, L. Sun, T. Nguyen, Langmuir 24 (2008) 3867.
[21] K. Peng, A. Lu, R. Zhang, S. Lee, Adv. Funct. Mater. 18 (2008) 3026.
[22] S. Lee, J.H. Koo, J. Seo, S.-D. Kim, K.H. Lee, S. Im, Y.-W. Kim, T. Lee, J. Nanopart. Res 14 (2012) 840.
[23] J. Seo, H. Lee, S. Lee, T.I. Lee, J.-M. Myoung, T. Lee, Small 8 (2012) 1614.
[24] K. Peng, J. Hu, Y. Yan, Y. Wu, H. Fang, Y. Xu, S. Lee, J. Zhu, Adv. Funct. Mater. 16 (2006) 387.
[25] L. Zhang, D.E. Resasco, Langmuir 25 (2009) 4792.
[26] N.A. Patankar, Langmuir 20 (2004) 8209.
[27] M.M. Moslehi, S.C. Shatas, K.C. Saraswat, Appl. Phys. Lett. 47 (1985) 1353.
[28] S.A. Schafer, S.A. Lyon, Appl. Phys. Lett. 47 (1985) 154.
[29] B.E. Deal, M. Sklar, A.S. Grove, E.H. Snow, J. Electrochem. Soc. 114 (1967) 266.
[30] M. Revitz, S.I. Raider, R.A. Gdula, J. Vac. Sci. Technol. 16 (1979) 345.
[31] C.-M. Chiang, B.R. Zegarski, L.H. Dubois, J. Phys. Chem. 97 (1993) 6948.
[32] B. Bhushan, in: Springer handbook of nanotechnology, Springer-Verlag, Berlin Heidelberg, 2004, p. 877.
[33] L.T. Zhuravlev, Colloids Surf. A 173 (2000) 1.
[34] R.K. Iler, in: The chemistry of silica solubility, polymerization, colloid and surface properties, and biochemistry, Wiley-Interscience, New York, 1979, p. 866.
[35] P. Hoffmann, E. Knözinger, Surf. Sci. 188 (1987) 181.
[36] O. Sneh, M.A. Cameron, S.M. Geroge, Surf. Sci. 364 (1996) 61.
[37] N. Sato, T. Yonehara, Appl. Phys. Lett. 65 (1994) 1924.
[38] H. Kuribayashi, R. Hiruta, R. Shimizu, K. Sudoh, H. Iwasaki, J. Vac. Sci. Technol. A 21 (2003) 1279.
[39] R.K. Iler, in: The chemistry of silica, Wiley-Interscience, New York, 1979, p. 622.
[40] T. Kudo, S. Nagase, J. Am. Chem. Soc. 107 (1985) 2589.
[41] B.C. Bunker, D.M. Haaland, K.J. Ward, T.A. Michalske, W.L. Smith, J.S. Binkley, C.F. Melius, C.A. Balfe, Surf. Sci. 201 (1989) 406.
[42] D.J. Michalak, S.R. Amy, D. Arueau, M. Dai, A. Estève, Y.J. Chabal, Nat. Mater. 9 (2010) 266.